Received: 4 September 2023 | Revised: 8 October 2023 | Accepted: 22 October 2023

DOI: 10.1002/appl.202300080

Applied Research

MINI REVIEW

Recent advances in cocatalyst engineering for solar-driven overall water splitting

Christian Mark Pelicano | **Haijian Tong**

Department of Colloid Chemistry, Max Planck Institute of Colloids and Interfaces, Potsdam, Germany

Correspondence
Christian Mark Pelicano, Department of Colloid Chemistry, Max Planck Institute of Colloids and Interfaces, Am Mühlenberg 1, 14476 Potsdam, Germany.
Email: christianmark.pelicano@mpikg.mpg.de

Abstract

Solar-driven overall water splitting using particulate photocatalysts represents a viable and attractive paradigm to produce H_2. To achieve sustainable artificial photosynthesis, considerable effort has been devoted in enhancing the overall efficiency and stability of photocatalysts. More specifically, modifying the photocatalyst surface with suitable cocatalysts can significantly enhance its water-splitting performance. In this minireview, we describe recent advances with respect to the hybridization strategies in constructing high-performance cocatalyst/photocatalyst systems. We first discuss the fundamental concepts and principles governing the photocatalytic water splitting and the important role of cocatalysts. Subsequently, we examine the strengths and drawbacks of conventional and emerging cocatalyst loading strategies. Special consideration is given to the structure–activity relationship of cocatalysts to achieve efficient photocatalytic H_2 production from pure H_2O. Finally, the remaining key challenges and possible future directions in the discovery and further exploration of cocatalyst materials are also discussed. We anticipate this review will provide insights and inspire more research interest in designing high-performance cocatalysts for photocatalytic overall water splitting.

KEYWORDS

cocatalyst, hybridization, hydrogen, overall water splitting, photocatalysis

INTRODUCTION

Resolving the constantly increasing global energy requirement through carbon-neutral energy sources is among the most serious challenges in recent times [1]. Solar-driven photocatalytic H_2O splitting has been considered as one of the best strategies for producing H_2 (Figure 1a). Although storage of H_2 presents a number of technical challenges, it is still regarded as a favorable energy carrier and a reactant for CO_2 reduction [2]. When used as a carbon-free fuel, it only releases zero emission and produces H_2O as by-product upon its combustion. In comparison to other solar-hydrogen methods (e.g., photoelectrocatalysis and photovoltaic electrolysis) [3–6], the decomposition of H_2O via particulate photocatalysis could be readily scaled-up in a cost-effective manner. Extensive research has been directed in designing high-performance photocatalyst systems and the working mechanism has been examined exhaustively over the past decades. In fact, a recent field-scale experiment has established the practical viability of photocatalytic overall water splitting (OWS), wherein a photocatalytic solar panel reactor with an area of 100 m^2 was developed without loss of efficiency over a span of several months [7]. However, current solar-to-hydrogen (STH) energy conversion efficiencies are still far from the target 5%–10% range to make solar-driven H_2 production via OWS economically feasible.

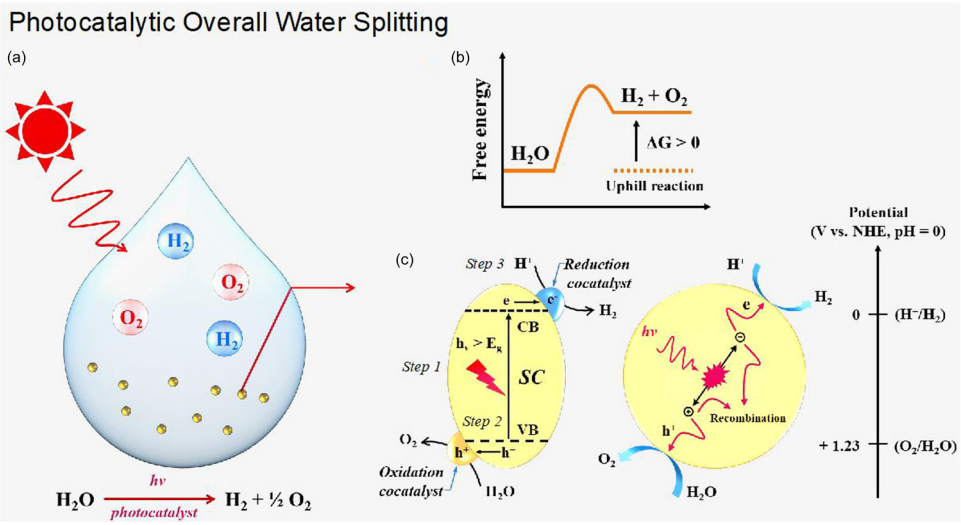

FIGURE 1 (a) Solar-driven H_2 generation from pure H_2O using particulate photocatalysts. (b) Energy requirement, and (c) schematic illustration of OWS on a photocatalytic semiconductor. OWS, overall water splitting.

Water splitting is an unfavorable uphill reaction (Figure 1b) with a large positive Gibbs free energy change of 237 kJ mol^{-1} at 298 K [8], as shown in Equation (1):

$$H_2O \rightarrow H_2 + ½O_2. \quad (1)$$

Hence, an external energy is required in order for this reaction to proceed, which solar energy can supply. This research has received widespread attention and has been regarded as the "holy grail" in photochemistry community since Fujishima discovered that a single-crystal TiO_2 photoelectrode can decompose water [9]. The production of H_2 and O_2 on a semiconductor photocatalyst involves three essential steps (Figure 1c): (1) the absorption of photons with energy values equal to or higher than the semiconductor band gap ($h\nu \geq E_g$) to excite electrons from the valence band to the conductive band and leaving holes on the valence band; (2) separation of photogenerated electrons and holes and subsequent migration to the active sites of the photocatalyst surface; and (3) promotion of the redox reactions to produce H_2 and O_2 with the aid of the cocatalysts. The reactions are summarized through the following equations below [10].

Hydrogen evolution (HER):

$$2H^+ + 2e^- \rightarrow H_2 \text{(acidic conditions)}, \quad (2)$$

$$2H_2O + 2e^- \rightarrow H_2 + 2H^- \text{(alkaline conditions)}. \quad (3)$$

Oxygen evolution reaction (OER):

$$2H_2O \rightarrow O_2 + 4e^- + 4H^+ \text{(acidic conditions)}, \quad (4)$$

$$4OH^- \rightarrow O_2 + 4e^- + 2H_2O \text{(alkaline conditions)}. \quad (5)$$

To initiate OWS, the valence band maximum must be more positive than the H_2O/O_2 oxidation potential (+1.23 V vs. NHE, pH = 0) and the conductive band minimum must be more negative than the H^+/H_2O reduction potential (0 V vs. NHE, pH = 0) [11]. Therefore, the minimum light energy necessary to drive OWS is 1.23 eV and this makes the utilization of the full visible-light range ($400 < \lambda < 800$ nm) possible. Nevertheless, supplemental kinetic overpotentials are normally needed to drive the carrier transfer step and the water-splitting reactions at acceptable rates. Considerable efforts have been mainly focused in designing photocatalysts with extended light absorption (step 1) along with an efficient charge separation and migration (step 2). In particular, a range of strategies have been developed to improve the photonic efficiencies of photocatalytic systems including valence band engineering [12], doping [13], quantum dots [14], dye-sensitization [15], heterostructure formation [16], and Z-scheme construction [17]. On the other hand, diverse nanostructured semiconductor photocatalysts with high crystallinity and shorter charge diffusion length have been examined to realize superior charge separation and transport [18–20].

Role of cocatalysts on photocatalytic overall water splitting

Most photocatalysts do not possess the catalytic capacity to facilitate proton reduction and/or water oxidation reactions. As a consequence, semiconductors are modified with electrocatalysts, often called cocatalysts, to promote these reactions. As discussed earlier, the third step to achieve OWS is facilitated by H_2-evolution and O_2-evolution cocatalysts, which serve as active sites by lowering their respective overpotentials [21, 22]. This is especially critical for O_2-evolution reaction which involves a four-electron and four-proton pathway and requires a large thermodynamic potential. As a result, the application of O_2-evolution cocatalyst with small overpotential could augment the OWS efficiency. Moreover, cocatalysts can aid the electron-hole pair separation. As shown in Figure 1c, the photoexcited electrons are captured by reductive cocatalyst and reduce H^+ to H_2 while the holes are trapped by oxidative cocatalyst and oxidize H_2O to generate O_2.

It is noteworthy that a finely tuned interface between the photocatalyst and cocatalyst is a prerequisite for an effective carrier separation and migration. Most importantly, the energy level alignment at the interface should be suitable to establish an Ohmic contact or reduce the barrier height to maximize the photogenerated carrier usage. Likewise, an intimate heterojunction is notably advantageous to suppress charge recombination and improve the efficiency. Cocatalyst can also inhibit the photocorrosion of the photocatalysts and in turn enhance their long-term stability and durability. Normally, visible-light responsive photocatalysts including (oxy)nitrides and (oxy) sulfides are not stable in H_2O oxidation, since the anions are more susceptible to oxidation than H_2O [23, 24]. Thus, hybridizing semiconductor photocatalysts with cocatalysts could prevent their decomposition by capturing the photoexcited holes for H_2O oxidation. Moreover, a volcano-type correlation between the amount of cocatalyst loaded and the photocatalytic performance is commonly observed irrespective of the type of cocatalysts and photocatalysts employed (Figure 2) [8]. As noted previously, modifying photocatalyst with cocatalyst lessens charge recombination and enhances reaction kinetics, thereby augmenting the photocatalytic activity. However, a severe reduction in activity occurs once an excess of cocatalysts have been immobilized as they can shield the semiconductor surface from the incident light and concurrently serve as recombination sites.

In recent years, a number of reviews focusing on specific materials that can be used as cocatalysts have been presented such as earth-abundant cocatalysts [8], transitional metal disulfide [25], and bimetallic nanoparticles [26]. However, no related work has given an in-depth and comprehensive discussion on cocatalyst engineering strategies for photocatalytic OWS, hence, a concise review is essential to propel further advances in this important catalysis field. In this minireview, we examine the significant progress that has been achieved in developing cocatalyst materials and how to effectively construct intimate cocatalyst/photocatalyst interface. More specifically, we highlight the advantages of each hybridization strategy and their suitability for specific materials. A special attention is put on the cocatalyst engineering strategies recently applied to realize photocatalytic H_2 production in pure H_2O. Finally, we outline the challenges and outlook by giving a preview of potential directions for further advancement of cocatalyst performance.

GENERAL COCATALYST LOADING SCHEMES

Hybridization between a photocatalyst and cocatalyst plays a crucial role in achieving the optimal photocatalytic performance of the system. More specifically, the synthetic routes for cocatalysts determine their size, structure, and dispersion which have a great effect on the activity of the hybrid material. In general, cocatalysts can be in-situ/directly (e.g., impregnation, photodeposition, chemical reduction, etc.) or ex-situ/sequentially deposited (liquid-phase adsorption, mechanical mixing, electrostatic self-assembly, etc.) onto the semiconductor. Direct hybridization refers to the methods in which cocatalysts are simultaneously formed from the precursors on the photocatalyst surface.

This strategy ensures the creation of sufficient and an intimate cocatalyst/photocatalyst interfacial contact, thereby promoting photoexcited carrier separation and transport. However, direct coupling of cocatalysts with photocatalyst largely depends on the overall stability of

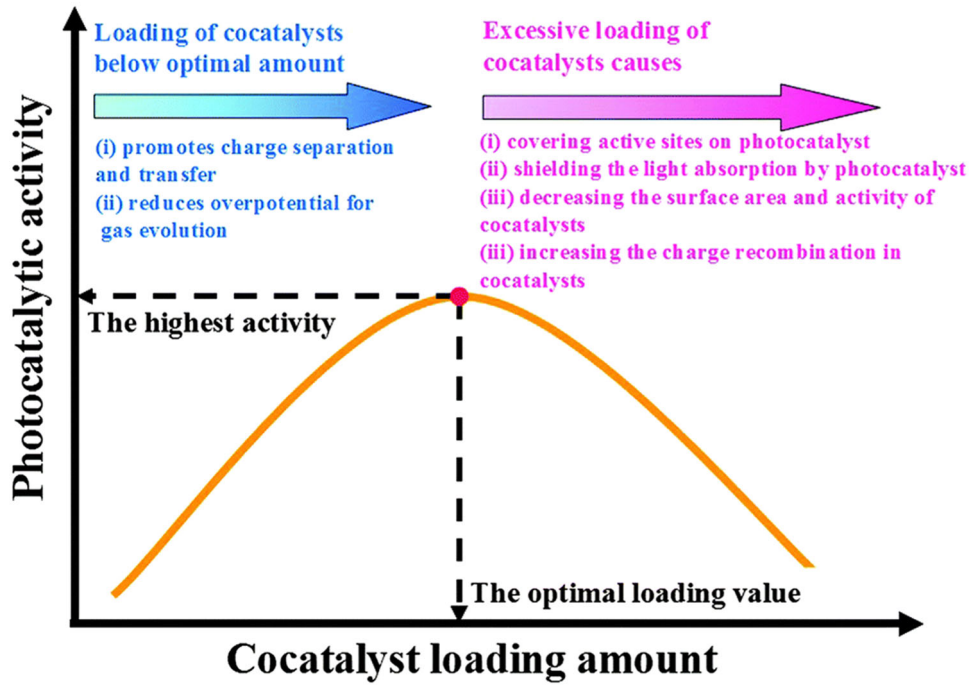

FIGURE 2 An illustration of volcano-type relationship between the amount of cocatalyst loading and the photocatalytic performance of a semiconductor photocatalyst modified with cocatalysts. Reproduced with permission [8], Copyright 2014, The Royal Society of Chemistry.

the photocatalyst. Likewise, the control over the cocatalyst size and composition are challenging due to the presence of photocatalysts during cocatalyst deposition. On the other hand, ex-situ deposition permits the immobilization of presynthesized cocatalyst particles on the substrate. Here, the particle size and chemical composition of the cocatalysts can be easily precontrolled to maximize their catalytic activities. Conversely, the resulting interfacial contact between the cocatalyst and semiconductors using ex situ deposition routes are at times unsatisfactory and therefore must be thoroughly optimized via thermal processing methods. In this context, the application of ligands or surfactants to enhance the interfacial coupling within the hybrid would be desirable followed by their removal through high-temperature annealing. Another way to induce a compact contact area is to take advantage of conductive binders. Ex-situ hybridization is also advantageous in assembling 2D-2D layered heterostructure of cocatalysts and photocatalysts. Finally, indirect coupling likewise enables a quantitative evaluation of the electrocatalytic activities of cocatalysts by performing electrochemical characterizations without the photocatalysts. In this section, we describe the advantages and shortcomings of traditional and emerging cocatalyst loading strategies (Table 1).

Direct hybridization

Impregnation

One of the simplest cocatalyst deposition procedure is the impregnation method. Typically, precursor solution is uniformly dispersed over the semiconductor substrate and solvent is then completely removed by drying. Then the impregnated metal precursors are subsequently annealed under oxidizing or reducing conditions to transform them into active nanoparticulate cocatalysts (Figure 3a). A range of solvents and precursors can be chosen for this approach in conjunction with the succeeding treatment conditions. Domen et al. first demonstrated the loading of NiO_x nanoparticles onto the surface of $SrTiO_3$ via impregnation in 1980 [27]. After four decades, the same group reported a 1 m^2-size photocatalytic water-splitting panel with an STH of 0.4% using impregnated $RhCrO_x$ cocatalyst on $SrTiO_3$:Al photocatalyst [28]. A recent study by Xue et al. reported the formation of Co_xNi_yP cocatalyst by impregnating Co and Ni precursors onto graphitic carbon nitride and followed by a high-temperature phosphorization process (Figure 4a–c), which validates the possibility of immobilizing not only metal or metal oxides but also phosphide-based cocatalysts [29]. Nevertheless, the major drawback of the impregnation technique is the application of high-temperature annealing for cocatalyst activation, limiting the availability of photocatalyst materials that are not thermally stable. Previous reports have similarly indicated that regulating cocatalyst dispersion and size distribution is difficult to achieve through this method and aggregation of cocatalysts may negatively affect their catalytic activities [36]. The aggregation is especially drastic for non-noble transition metal catalysts (e.g., Ni, Cu, Co, etc.) which have to be supported at a high loading (normally, 10–30 wt%) to compete with noble metals [37, 38].

Photodeposition

Another traditional cocatalyst deposition method is the light-assisted chemical reduction (or photochemical reduction). By irradiating light to an aqueous solution containing metal ions and semiconductor support, photoexcited carriers migrate to the semiconductor surface and reduce/oxidize the proper precursors leading to the formation and immobilization of particulate cocatalysts (Figure 3b) [40]. Assuming that the photon energy is sufficient to excite the semiconductor, the conduction band minimum (or LUMO) must be more negative than the reduction potential of reductive cocatalyst, and the valence band maximum (or HOMO) must be more positive than the oxidation potential of oxidative cocatalyst to trigger photochemical deposition. An attractive feature of photodeposition is the site-selective loading of reduction and oxidation cocatalysts on the electron-rich and hole-rich facets of the photocatalyst, respectively [41]. As a result, the shorter carrier route from the

TABLE 1 Summary of the hybridization methods for various photocatalysts and cocatalysts.

Photocatalyst	Cocatalyst	Type of cocatalyst	Hybridization method	References
$SrTiO_3$	NiO_x	HER	Impregnation	[27]
$SrTiO_3$:Al	$RhCrO_x$	HER	Impregnation	[28]
g-C_3N_4	Co_xNi_yP	HER	Impregnation + Phosphorization	[29]
$SrTiO_3$	Pt, Au, and Ag	HER	Photodeposition	[30]
$SrTiO_3$	MnO_x and Co_3O_4	OER	Photodeposition	[30]
TiO_2/CdS	Pt	HER	Chemical Reduction	[31]
g-C_3N_4	Ni_xCo_yP@C	HER	Ball milling	[32]
rGO/$La_2Ti_2O_7$	NiFe-LDH	HER	Ultrasonication	[33]
GaN:ZnO	Rh	HER	Liquid-phase adsorption	[34]
$SrTiO_3$:Al	PtRu	HER	Liquid-phase adsorption	[35]

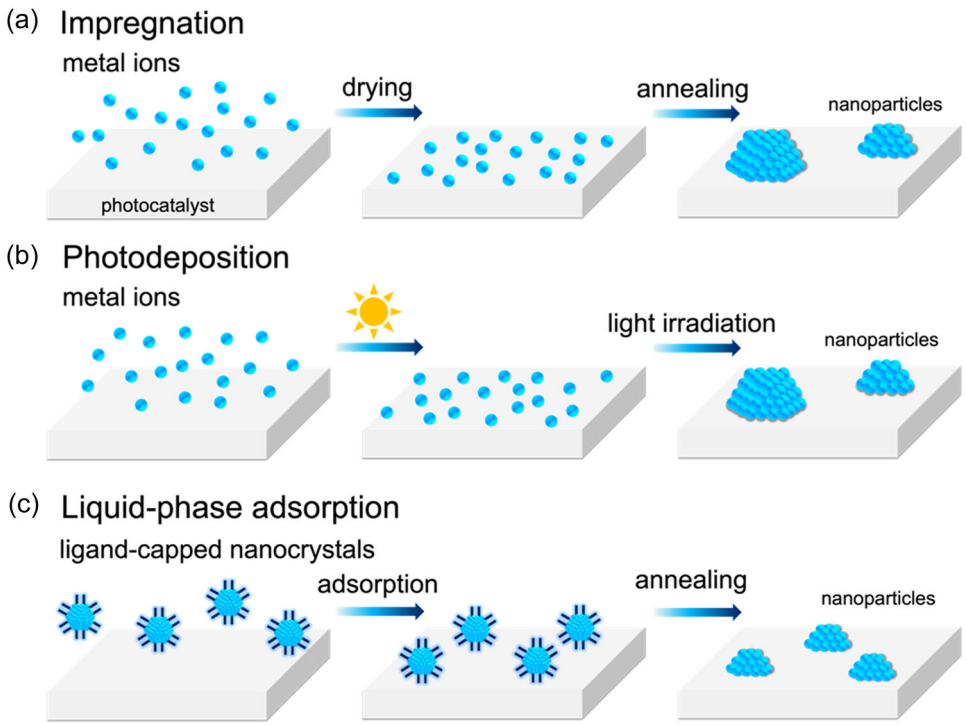

FIGURE 3 Schematic illustrations of (a) impregnation, (b) photodeposition, and (c) liquid-phase adsorption loading methods.

semiconductor to the cocatalyst enhances charge separation and simultaneously suppresses recombination. Li et al. have reported the dual cocatalyst deposition of reduction (Pt, Au, and Ag) and oxidation (MnO_x and Co_3O_4) cocatalysts on the {001} and {110} planes of an 18-facet $SrTiO_3$ nanocrystal, which resulted in a 5-fold enhancement in apparent quantum yield for OWS (Figure 4d,e) [30]. In comparison to other alternative loading schemes that involve elevated temperature/pressure, applied potential, and presence of redox reagents, photodeposition only requires illumination to form well-defined cocatalysts and enables the utilization of thermally unstable photocatalysts [42, 43]. Other favorable attributes of this process include control over the structure, composition, distribution, and oxidation state of the cocatalysts. Apart from (noble and transition) metals [44–46] and metal oxides [47–49], materials based on metal sulfides [50–52], metal (oxy)hydroxides [53–55], metal phosphates [56, 57], metal phosphides [58, 59] can be photodeposited as either H_2- or O_2-evolution cocatalysts.

Chemical reduction

This method allows the rapid deposition of metal nanocrystals on the photocatalyst surface from their related organic or ionic metal precursors. In particular, metal ions are first adsorbed and then reduced to metal nanoparticles by a reducing agent with the aid of a stabilizer. Standard chemical reduction protocols involve reducing the metal salt precursors as a solid at high temperature under reducing atmosphere [39, 60] or in solution phase by soluble or liquid reductants that can also function as solvents such as ethylene glycol [61], $NaBH_4$ [62], and hydrazine hydrate [63]. For example, Ning et al. described the formation of metallic Pt nanoparticles from the reduction of H_2PtCl_6 solution by hydrazine hydrate over a TiO_2/CdS photocatalyst for OWS (Figure 4f–h) [31]. By choosing suitable surfactants or ligands, diverse metal nanoparticles with well-defined structures, sizes, and shapes can be synthesized even in the presence of photocatalyst particles.

Ex-situ deposition

Mechanical mixing

Mechanical mixing is the simplest way of constructing a cocatalyst/photocatalyst hybrid system. Ball milling is a well-established technique to homogenously mix two or more solid materials in large scale [64, 65]. This process requires minimal to no solvent and can be applied for a wide variety of photocatalysts [66]. A supplementary annealing treatment is necessary to reinforce the interface between the cocatalyst and the substrate. Zhang et al. successfully coupled Ni_xCo_yP@C cocatalyst with g-C_3N_4 photocatalyst via ball milling and achieved a comparable photocatalytic H_2 evolution performance with Pt-modified g-C_3N_4 (Figure 5a–c) [32]. Another facile approach to physically mix photocatalysts with cocatalysts is through ultrasonication. Recently, a ternary rGO/$La_2Ti_2O_7$/NiFe-LDH nanosheets were constructed using ultrasound-assisted electrostatic self-assembly method [33]. The heterostructure displayed superior photocatalytic

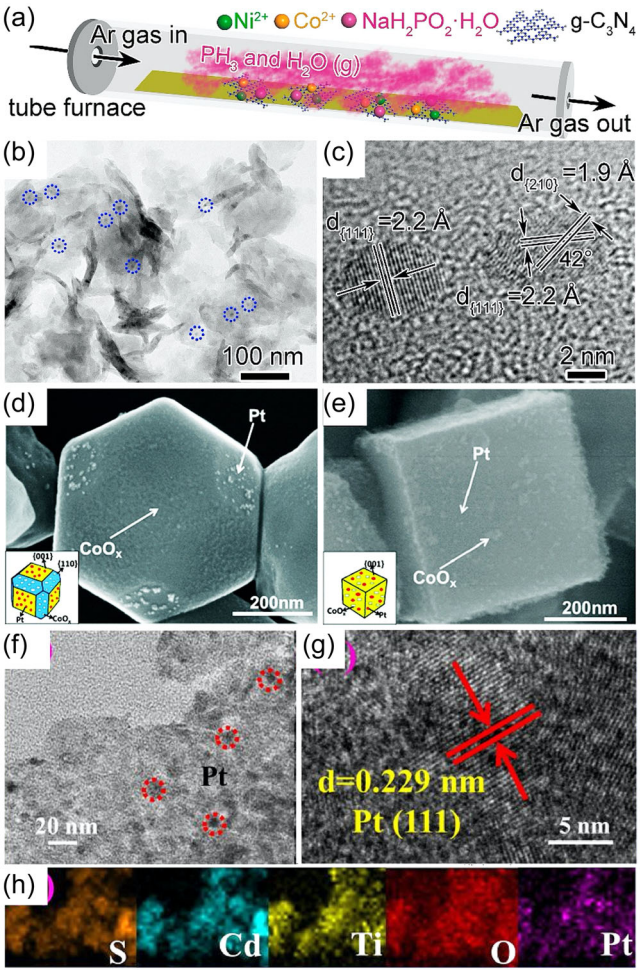

FIGURE 4 (a) Schematic illustration showing the fabrication of Co_xNi_yP via impregnation and subsequent phosphorization on g-C_3N_4 photocatalyst. (b) TEM and (C) HRTEM images of Co_xNi_yP cocatalysts on g-C_3N_4. Reproduced with permission. [29] Copyright 2019, Elsevier. SEM images of the 18-facet and 6-facet $SrTiO_3$ nanocrystals with simultaneous photodeposition of Pt and Co_3O_4 as cocatalysts. (D) Pt–Co_3O_4/18-facet $SrTiO_3$ and (E) Pt–Co_3O_4/6-facet $SrTiO_3$. Reproduced with permission. [35] Copyright 2016, The Royal Society of Chemistry. (F) TEM, (G) HRTEM, and (H) elemental mapping images of Pt-TiO_2/CdS photocatalyst. Reproduced with permission. [39] Copyright 2017, Elsevier. HRTEM, high-resolution transmission electron microscopy.

H_2 generation relative to its components, highlighting the potential of ultrasonication of creating effective interface for high-performance photocatalysis.

Liquid-phase adsorption

The high level of control over chemical composition, shape, and size in colloidal nanocrystals makes them invaluable as cocatalysts for highly active water-splitting systems. Recent advances in the preparation of colloidal crystals can offer an attractive way to normalize their properties even to the level of atomically-precise nanoparticles [67]. In liquid-phase adsorption process, colloidal nanocrystals are attached on the photocatalyst surface via stirring in a solvent. Considering that photocatalysts may have surface hydroxyl groups (–OH), ligand-capped nanocrystals containing functional groups can be adsorbed onto the photocatalyst surface through hydrogen bonding [68]. A subsequent ligand removal (e.g., calcination or ozone oxidation) is required since organic molecules may act as recombination sites for photoexcited carriers. In 2009, Domen et al. introduced the application of monodispersed colloidal Rh nanoparticles as cocatalysts for GaN:ZnO solid solution photocatalyst system for OWS [68]. A follow-up study identified the influence of particle size of Rh nanoparticles on the water-splitting performance [34].

Furthermore, this strategy allows a quantitative understanding of the electrocatalytic activities of similar nanoparticulate cocatalysts by conducting isolated electrochemical analyses. For example, Teranishi et al. have synthesized ultrafine bimetallic alloy nanoparticles via a polyol method and revealed that alloying Pt with Ru enhanced the electrocatalytic H_2 evolution and reduced the O_2 reduction reaction activities of Pt (Figure 5d–h) [35]. By applying the knowledge gained from electrocatalysis, the optimal PtRu nanoparticulate electrocatalysts were integrated onto Al-doped $SrTiO_3$ via liquid-phase adsorption as H_2-evolution cocatalysts. With the co-loading of CoOOH nanoparticles as O_2-evolution cocatalysts, this system reached an apparent quantum yield of 65% at 365 nm, which is the most efficient for $SrTiO_3$-based photocatalytic OWS with Rh-free cocatalyst. These results make liquid-phase adsorption an emerging scheme in loading precisely controlled cocatalysts to photocatalysts.

COCATALYST ENGINEERING STRATEGIES FOR OVERALL PHOTOCATALYTIC WATER SPLITTING

Morphological and structural engineering

The size of the cocatalysts has a prominent role on the photocatalytic OWS activity. Smaller cocatalysts have larger surface area and offer a higher number of active sites given the same loading amount, which leads to a higher catalytic performance. Additionally, they could not limit light absorption by photocatalysts owing to their small size. For instance, a previous study prepared a series of Rh nanoparticles via a polyol reduction using polyvinylpyrrolidone as a surfactant. By varying the reaction pH and temperature, monodisperse Rh nanoparticles with different sizes were fabricated. It was found that applying smaller Rh nanoparticles as cocatalysts could boost the water-splitting performance of GaN:ZnO photocatalysts (Figure 6a) [34]. There is also a higher chance of suppressing the charge recombination using cocatalysts with smaller sizes than the larger ones. Smaller nanoparticulate cocatalysts might as well demonstrate lower barriers for interfacial charge transfer from photocatalysts. Indeed, many reports have confirmed that ultrafine nanoparticulate cocatalysts with high dispersion results in an improved photocatalytic efficiency [69–73]. However, there are cases that size reduction in cocatalysts show adverse effects on the catalytic performance. When Pt nanoparticles reach the size of <2 nm, their

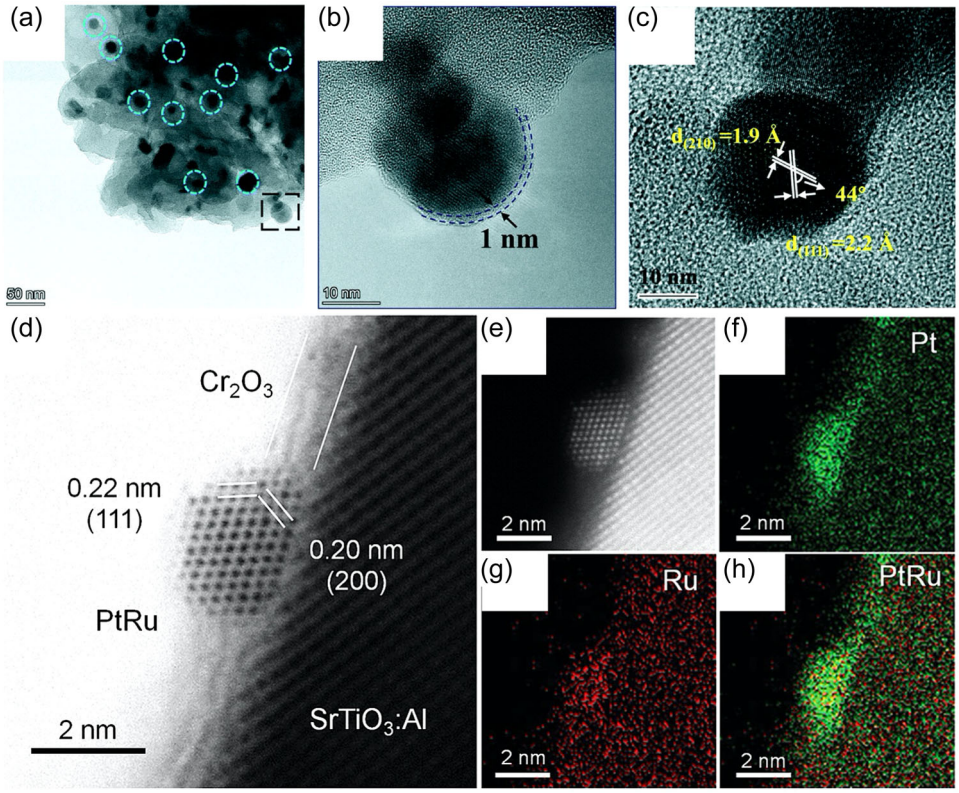

FIGURE 5 (a–c) HRTEM images of Ni_3Co_7–P@C/CN photocatalyst prepared via ball-milling. Reproduced with permission. [63] Copyright 2022, The Royal Society of Chemistry. (d) BF–STEM and (e) HAADF–STEM images of air–H_2–PtRu/$SrTiO_3$:Al coated with Cr_2O_3. (f, g) Pt and Ru STEM–EDX maps and (h) overlay images of (f) and (g). BF-STEM, bright-field scanning transmission electron microscopy; HAADF, high-angle annular dark-field imaging; HRTEM, high-resolution transmission electron microscopy.

surface appears to have less-active edge sites lowering their activity towards the electrocatalytic H_2 evolution [74–76]. A density functional theory (DFT) calculation showed that the surface of larger metallic Pt has proper H^* adsorption energy for H_2 evolution, whereas sizes smaller than 1 nm has less-metallic characteristics which can promote electron transfer from TiO_2 [77]. This work suggests that an optimal cocatalyst size should be determined to achieve the equilibrium between the surface reaction kinetics and electron transfer efficiency [78]. Apart from size, the shape of cocatalysts apparently likewise determines the activity trend. To explore the influence of the shape of Pt nanoparticles as cocatalysts [79], Cao et al. loaded cubic, octahedral, and spherical Pt nanoparticles on g-C_3N_4 photocatalysts. As illustrated in Figure 6b, spherical Pt-loaded g-C_3N_4 revealed the highest activity among the samples. This is due to the fact that a spherical Pt nanoparticle consists of numerous {100} and {111} facets which have substantial quantity of edges at the interfaces and endowed with more active sites.

Compositional engineering is a straightforward strategy to tune the activity of cocatalysts. For example, bimetallic alloy systems can modify their geometric and electronic structures which can induce unprecedented properties that are far superb than their monometallic parents [80, 81]. Domen et al. successfully modified $SrTaO_2N$ photocatalyst with $RuIrO_x$ cocatalysts for OWS [82]. By incorporating Ru to IrO_2-loaded $SrTaO_2N$ via a conventional impregnation-thermal reduction process, the formed $RuIrO_x$ cocatalyst promoted charge separation and accelerated surface reactions (Figure 6c–h). Besides, the most active cocatalysts for evolving H_2 and O_2 gases are based on noble metals (e.g., Rh, RuO_2, and IrO_2). Needless to say, these metals are expensive and unsustainable for practical application. Hence, the development and exploration of cost-effective cocatalysts with analogous activity as with the noble metals are highly desirable and urgent matter. In recent years, novel cocatalysts prepared from earth-abundant elements have been developed to facilitate photocatalytic OWS. Zong et al. synthesized CoP as active site Al-doped $SrTiO_3$ for photocatalytic OWS [83]. CoP was hybridized onto the surface of the photocatalyst via in-situ photodeposition-phosphorization method. This cocatalyst has a metallic character and reduced the overpotential for H_2 production and at the same time accelerated the charge separation and migration. Other multi-component inorganic electrocatalysts such as perovskites, mixed-metal oxides, and spinels can be explored as cocatalysts for photocatalytic water splitting.

Suppression of reverse reactions

It is important to note that noble metals are unable to solely operate as cocatalysts for OWS. Although they provide efficient H_2 evolution sites, noble metals can also catalyze O_2 reduction reaction that

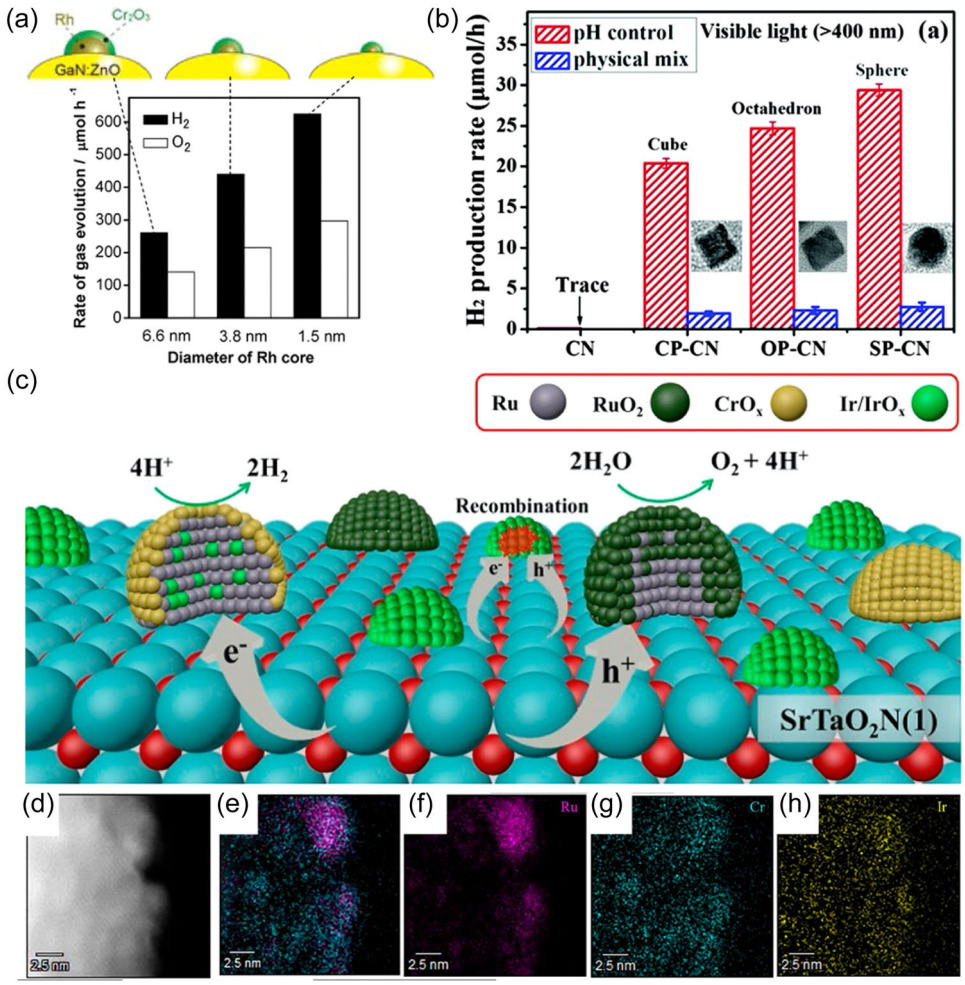

FIGURE 6 (a) Rates of H_2 and O_2 evolution over GaN:ZnO loaded with Rh@Cr_2O_3 core-shell nanoparticles. Reproduced with permission. [67] Copyright 2013, American Chemical Society. (b) Photocatalytic H_2 evolution activities of bare and Pt-loaded g-C_3N_4 photocatalysts under visible light. Reproduced with permission. [79] Copyright 2016, The Royal Society of Chemistry. (c) Illustration of the structure and dispersion of various cocatalysts on the surface of $SrTaO_2N$. (d) ADF-STEM image and (e–h) STEM-EDS elemental maps of the CrO_y/Ru/$IrO_{2(MW)}$/$SrTaO_2N$(1) specimen. Reproduced with permission. [82] Copyright 2023, American Chemical Society.

depletes evolved H_2 and O_2 during photocatalysis [68, 84, 85]. Thus, it is imperative to suppress the backward reaction to develop highly active photocatalyst systems. Maeda et al. first reported a prominent breakthrough to inhibit the reverse reaction by covering metal surfaces with Cr-based species [86]. From electrochemical and in situ in situ infrared reflection absorption spectroscopy (IRAS) analyses, it was established that the Cr-based layer (possibly $CrO_{(1.5-m)}(OH)_{2m}{\cdot}x$-$H_2O$) selectively permeate H^+ and H_2, but not oxygen atoms and molecules (Figure 7a) [87]. Up to now, the modification of cocatalysts with CrO_x has been exploited in diverse photocatalytic water-splitting systems such as GaN:ZnO [88], Al-doped $SrTiO_3$ [89], Ta_3N_5-nanorod [90], and visible-light responsive $Y_2Ti_2O_5S_2$ [91]. Similarly, the porous metal oxides such as SiO_x, lanthanide oxides, and MoO_x (Figure 7c,d) are identified to prevent the backward reaction during photocatalytic OWS [92, 93].

Another effective surface modification scheme in preventing the reverse reaction is through the photodeposition of amorphous oxyhydroxides of group IV and V transition metals (Ti, Nb, and Ta) over a cocatalyst/photocatalyst system [94]. By using metal peroxides as precursors, the photodeposition of metal oxyhydroxides over the whole photocatalyst surface created a core-shell structure (Figure 7b). Despite the fact that the active sites are fully covered, the selective permeation within the oxyhydroxide coating allowed H_2O to permeate in and the evolved gases to diffuse outward.

Site-selective dual cocatalyst deposition

As a central step in energy conversion, it is highly desirable to effectively separate the photogenerated electron-hole pairs and transferred to the photocatalyst surface for the target reactions. Normally, cocatalysts are randomly positioned over the photocatalyst which causes deactivation due to charge recombination. Thus, random cocatalyst deposition must be avoided and as presented earlier

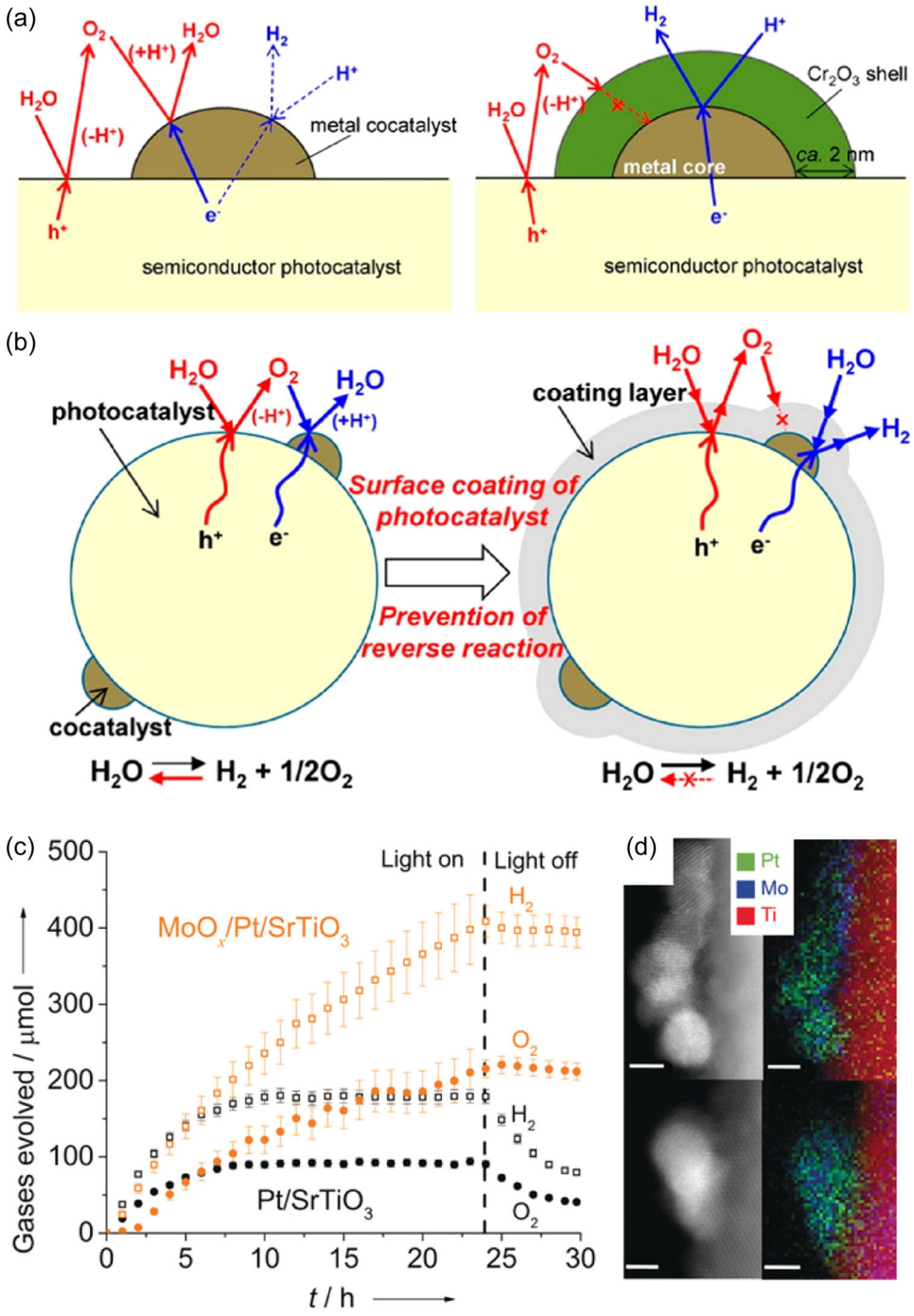

FIGURE 7 Schematic of the function of (a) a Cr_2O_3 shell and (b) reaction mechanism for OWS on a core–shell-structured photocatalyst. Reproduced with permission [94]. Copyright 2015, American Chemical Society. (c) Photocatalytic H_2 and O_2 evolution activities of 0.3 wt % Pt/$SrTiO_3$ with and without MoO_x under UV-light irradiation. (d) HAADF-STEM images of MoO_x/Pt/$SrTiO_3$ after photocatalysis and their corresponding elemental mappings (Scale bar: 2 nm). Reproduced with permission [92]. Copyright 2017, Wiley-VCH. OWS, overall water splitting.

photodeposition could be a strategic way to preferentially load metallic or metal oxide nanoparticles on desired redox locations. For this reason, spatial separation of reductive and oxidative sites is a sensible strategy to achieve a highly efficient photocatalytic water-splitting system [95]. When semiconductor photocatalysts are enclosed with multiple crystal facets, the work function difference between the planes triggers a potential gradient which results in the migration of electrons and holes on certain crystal planes [96, 97]. Accordingly, H_2- and O_2-evolution cocatalysts could be preferentially loaded on electron-rich and hole-rich facets, respectively (Figure 8a–c). Domen and his group perfected this approach to demonstrate OWS with an external quantum efficiency of up to 91.6% at an excitation

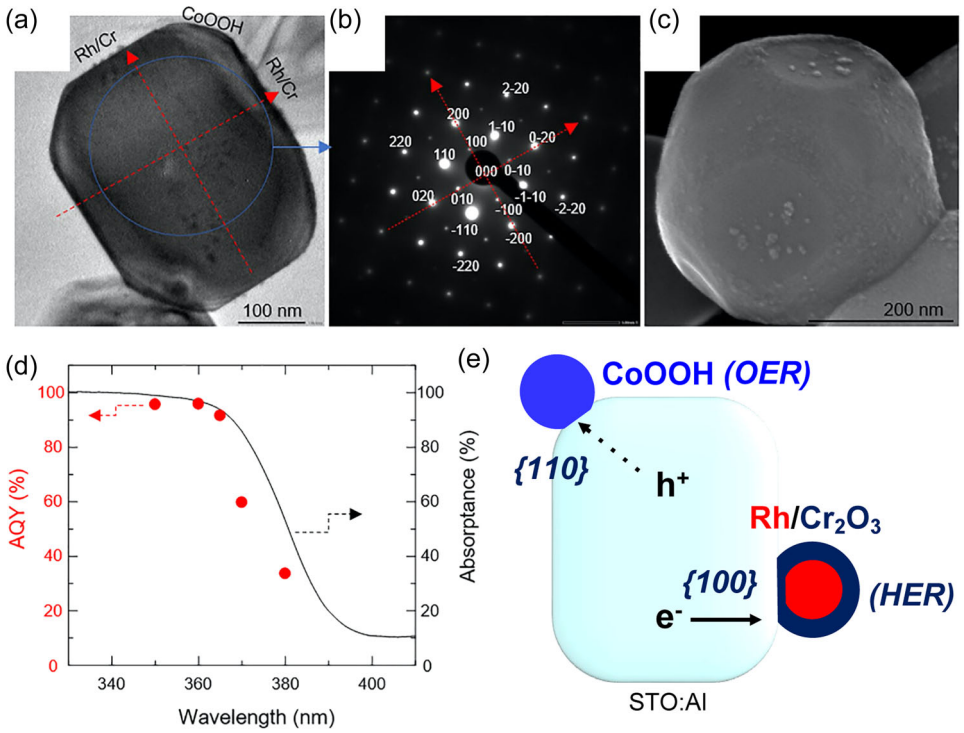

FIGURE 8 (a) TEM image, (b) SAED pattern, (c) SEM image, and (d) crystal orientation diagram for a $SrTiO_3$:Al/Rh@Cr_2O_3 + CoOOH photocatalyst system. (e) UV–visible diffuse reflectance spectrum (DRS) of bare $SrTiO_3$:Al and wavelength-dependent AQYs during OWS over $SrTiO_3$:Al/Rh@Cr_2O_3 + CoOOH photocatalyst system. Adapted with permission. [98] Copyright 2020, Springer Nature. OWS, overall water splitting; SEM, scanning electron microscope; TEM, transmission electron microscopy.

wavelength of 365 nm (Figure 8d) [97]. More specifically, Rh@Cr_2O_3 cocatalyst was reductively photodeposited as H_2-evolution cocatalyst on the {100} crystal facets, whereas CoOOH cocatalyst was oxidatively loaded as O_2-evolution cocatalyst on the {110} crystal facets of an Al-doped $SrTiO_3$ photocatalyst (Figure 8e). In turn, both cocatalysts were able to accelerate the succeeding charge separation and efficiently promote the redox reactions on their surfaces (Figure 9).

Active species determination via in situ/operando techniques

Monitoring the dynamic changes within the cocatalysts during photocatalytic reactions in real-time is crucial to elucidate the reaction mechanism, chemical behaviors, and structural evolution of cocatalysts, and eventually in designing superior cocatalysts [101, 102]. In situ and operando characterizations could bridge the gap between the structure and activity of cocatalysts under actual operating conditions by offering diverse environmental factors to mimic the actual reactions including light irradiation, atmosphere, temperature, and reactants. For example, Indra et al. applied in situ electron paramagnetic resonance (EPR) spectroscopy to uncover the nature of active Ni species during photocatalytic H_2 production [98]. As shown in Figure 10a, in situ EPR proved that the Ni^{2+} species are gradually reduced to metallic Ni during photocatalytic reaction and functions as a cocatalyst for proton reduction. Another study observed the structural changes of Pt active sites during photocatalytic OWS over PtO/TiO_2 using an operando X-ray absorption fine structure spectroscopy [99]. They found out that the coordination number and Pt–O bond length during OWS were altered in comparison to the precatalytic and postcatalytic stages. This important finding may serve as a guideline in developing highly active Pt-based cocatalysts. Spanu et al. investigated the composition and oxidation state of a bimetallic NiCu cocatalyst during photocatalytic H_2 production from ethanol-H_2O mixture via operando X-ray absorption spectroscopy [100]. The authors used a liquid-phase spectroscopic cell that simulated the working conditions during photocatalysis. The comparison between the oxidation states of Ni and Cu before and during UV irradiation revealed the formation of Ni and Cu metallic species from their oxides or hydroxides under light illumination. Simultaneously, an increase in the photocatalytic H_2 rate was observed which indicates that the metallic state of the cocatalysts caused the activity enhancement. Thus, it can be inferred that determining the active species plays a key role in augmenting surface reaction kinetics.

Theoretical design of high-performance cocatalysts

Catalytic activities and properties of materials are mainly associated with their electronic structures, and hence, their analyses necessitate computational techniques based on quantum mechanics [103].

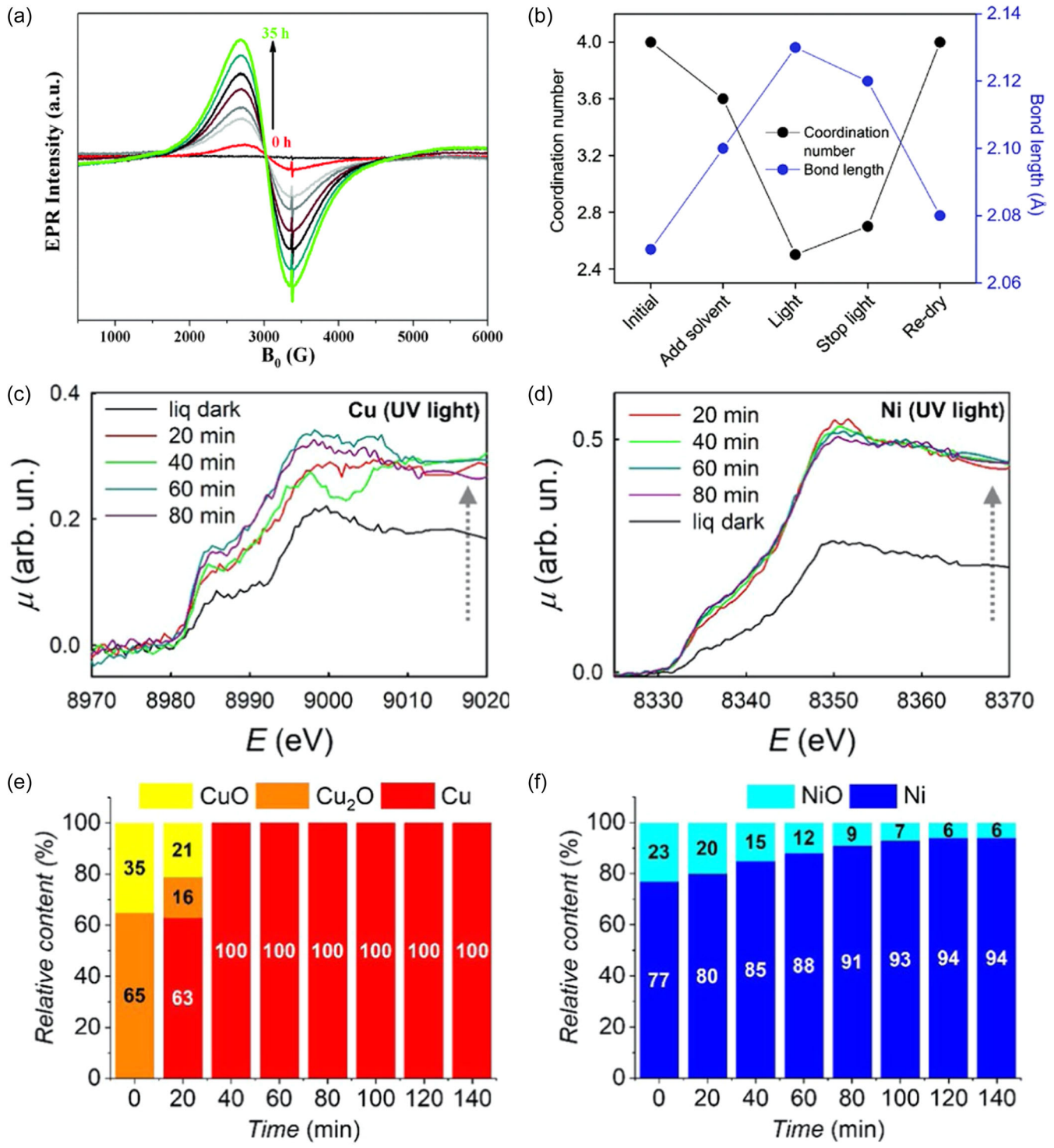

FIGURE 9 (a) In situ EPR examination of Ni-based cocatalyst on g-C_3N_4 during photocatalytic reaction. Reproduced with permission [98]. Copyright 2016, The Royal Society of Chemistry. (b) Coordination number and bond length of PtO cocatalyst at different experimental stages. Reproduced with permission [99]. Copyright 2017, The Royal Society of Chemistry. (c) Cu K-edge and (d) Ni K-edge XAS spectra of 5Ni5Cu–TiO_2 in a H_2O–ethanol under UV irradiation at different exposure times. (e) Cu and (f) Ni phase compositions determined by *operando* XAS for 5Ni5Cu–TiO_2. Reproduced with permission [100]. Copyright 2020, American Chemical Society.

Recent advances in theoretical calculations can enable a more efficient exploration and prediction of highly active cocatalysts. Traditional materials screening experiments for cocatalysts are often time-consuming and energy-intensive whereas density functional theory (DFT) calculations offer a faster approach for large-volume screening of cocatalysts for photocatalytic OWS [104]. Numerous studies on DFT calculations have aided in unraveling the structure–activity relationships and contributed in providing in-depth

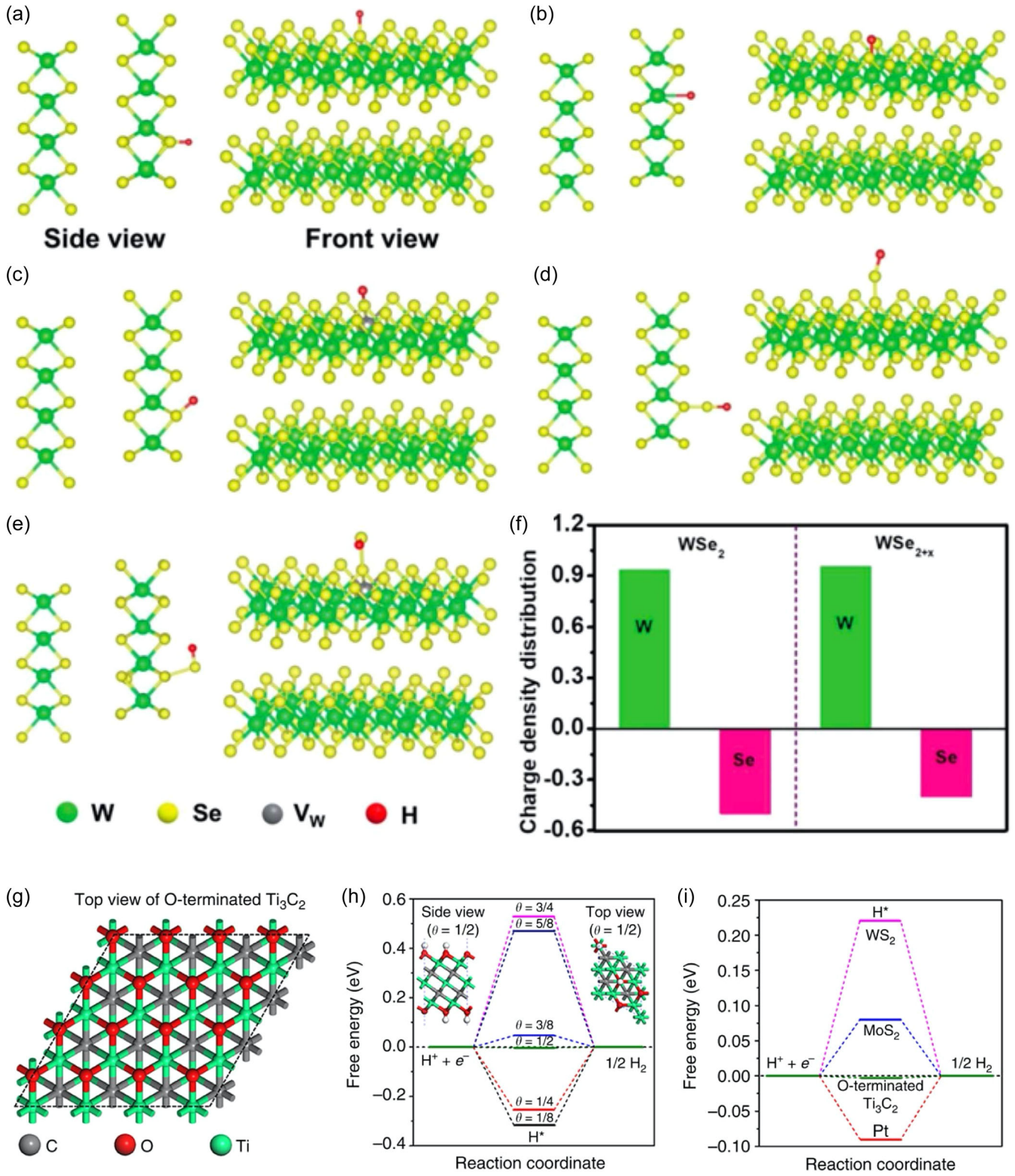

FIGURE 10 DFT calculation of unsaturated Se-enriched WSe_{2+x} nanodots cocatalyst, (a) hydrogen adsorption at Se sites, (b) W site, (c) Se site with W vacancy, (d) Se site with Se adhesion, (e) Se site with Se adhesion and W vacancy. (f) The charge density distribution in WSe_2 and unsaturated Se-enriched WSe_{2+x} nanodots. Reproduced with permission [105]. Copyright 2022, The Royal Society of Chemistry. (G) Top view of the structural model for a 4 × 4 × 1 O-terminated Ti_3C_2 supercell. (h) The calculated ΔG_{H^*} of HER at the equilibrium potential on the surface of a 2 × 2 × 1 O-terminated Ti_3C_2 supercell at various H* coverage conditions. (i) The calculated ΔG_{H^*} of HER at the equilibrium potential on the surface of O-terminated Ti_3C_2 supercell and reference Pt and MoS_2. Reproduced with permission [106]. Copyright 2017, Nature Publishing Group. DFT, density functional theory; HER, hydrogen evolution.

understanding of electronic behavior of cocatalyst materials. For example, Gao et al. unraveled the electronic state of electron-poor Se sites and their impact on strengthening Se-H_{ads} bonds by conducting first-principles calculations [105]. By loading Se-enriched WSe_{2+x} (3 wt%) nanodots on TiO_2 via a complexation–photodeposition strategy, an optimum H_2-evolution rate 3770.8 μmol h^{-1} g^{-1} is reached, which is 4.5 and 2.4-fold higher relative to crystalline WSe_2/TiO_2 and amorphous WSe_2/TiO_2, respectively. The Se-enriched WSe_{2+x} nanodots (0.5–1 nm) have abundant unsaturated Se atoms (45.8%) owing to their amorphous and unsaturated Se-enriched nature, which is much larger in comparison to amorphous WSe_2 (25.0%) and crystalline WSe_2 (8.6%). As such, usual (001) WSe_2 surface with Se and W terminals is optimized (Figure 10a–f). Unsaturated Se sites are generated through the W atom removal on the terminated (001) surface together with extra Se atom below to simulate the Se enrichment. Accordingly, Se atoms get less coordinated and become enriched in WSe_2, imitating an identical bonding in Se-enriched WSe_{2+x} nanodot cocatalysts.

The Bader charge further confirmed that the Se atom enrichment triggers an electron deficiency at Se sites in WSe_{2+x} cocatalyst in comparison to WSe_2 (Figure 10f). In turn, the creation of electron-poor $Se^{(2-\delta)-}$ sites promoted the adsorption of Hads for accelerated H_2 generation through the reinforcement of weak Se-H_{ads} bonds. Another important application of theoretical calculation is the estimation of the adsorption energies for the reactant and intermediate species on the surface of cocatalyst active sites [107]. Since cocatalysts are just electrocatalysts loaded on the photocatalyst surface, ΔG_{H^*} has been regarded as a main indicator of the H_2-evolution activity of cocatalyst materials (ΔG_{H^*} must be close to zero for optimal performance) [108]. For instance, a previous study examined the suitability of O-terminated Ti_3C_2 Mxene as a water-reduction cocatalyst [106]. They found out that the O-terminated Ti_3C_2 Mxene has a near-zero ΔG_{H^*} (0.00283 eV) at optimal H* coverage, which is more favorable that state-of-the-art Pt and earth-abundant HER catalysts such MoS_2 and WS_2. The hybridization of Ti_3C_2 Mxene and CdS photocatalyst led to a ultrahigh visible-light H_2 evolution activity of 14342 μmol $h^{-1}g^{-1}$ and an AQY of 40.1% at 420 nm. These above studies highlight the importance of theoretical calculations in gaining new insights for accelerated design of highly active cocatalysts.

SUMMARY AND OUTLOOK

Semiconductor photocatalysts lack the necessary active sites to drive water-splitting reactions, hence, hybridizing photocatalysts with cocatalysts is a classical approach to facilitate charge separation and transport. Furthermore, cocatalyst can not only function as photoexcited carrier sink but provide reaction sites as well as accelerate the intended redox reactions. In this minireview, we first discussed the conventional and emerging cocatalyst loading strategies. By highlighting the recent developments in hybridization schemes, the creation of high-performance cocatalyst/photocatalyst systems could be easily achieved. Since the activity equally depends on cocatalyst preparation and the ensuing cocatalyst/photocatalyst interface, cocatalyst engineering is essential in breaking the present limitations of water-splitting efficiency. An enhanced photocatalytic activity could be anticipated by precisely controlling the properties of cocatalysts such as size, composition, and dispersion on the photocatalyst surface. Since both H_2- and O_2-evolution sites occur on the same photocatalyst particle, it is highly desirable to spatially deposit reductive and oxidative cocatalysts to avoid charge carrier recombination and the reverse reaction. At the same time, cocatalyst materials also tend to intensify the rates of the backward reactions to the HER and OER (ORR and the HOR, respectively). These reverse reactions are undesirably more thermodynamically favorable than the forward reactions, thus, it is crucial to discriminately deactivate them. The most prevalent surface modification strategy is through coating the HER cocatalyst with Cr-based species. However, there are issues with the stability of CrO_x layer during OWS, for this reason, it is necessary to explore viable alternative materials for CrO_x. The development of earth-abundant cocatalysts as an alternative for noble metals could help in the shift of photocatalysis from lab-scale to industrial-scale production. Nonnoble metal-based cocatalysts are attractive since they possess good activities towards H_2 evolution and appropriate electrochemical selectivity. In fact, exploring highly efficient electrocatalysts as cocatalysts will speed up the search for the optimal material for H_2 and O_2 evolution reactions. Examining the intrinsic electrocatalytic activities of cocatalysts under the same photocatalytic conditions can provide crucial information on their real-time performance, chemical stability. Likewise, the long-term durability of cocatalysts must be realized since their deactivation might lead to corrosion of photocatalysts during reactions.

Another crucial concept that needs to be taken account when combining cocatalysts with photocatalysts is the energy level alignment between them. Notably, their Fermi levels or electronic structures must be regulated such that an effective junction (a Schottky-type or Ohmic-type) could be created and in which the charges flow to the appropriate direction. As stated in Section 3, applying isolated electrochemical measurements could aid in the optimization of cocatalyst activity and stability. The transformations of currently applied cocatalysts are not yet fully understood, thus, theoretical simulations and advanced characterizations techniques are important tools in understanding the real nature of the cocatalysts during photocatalysis. These analyses could be pivotal in determining the factors that affect cocatalyst performance and eventually in constructing highly active photocatalytic water-splitting systems.

CONFLICT OF INTEREST STATEMENT

The authors declare no conflict of interest.

DATA AVAILABILITY STATEMENT

Data sharing is not applicable to this article as no new data were created or analyzed in this study.

ORCID

Christian Mark Pelicano http://orcid.org/0000-0003-4119-2523

REFERENCES

[1] L. Lin, T. Hisatomi, S. Chen, T. Takata, K. Domen, *Trends Chem.* **2020**, *2*, 813.
[2] L. Li, X. Mu, W. Liu, Z. Mi, C.-J. Li, *J. Am. Chem. Soc.* **2015**, *137*, 7576.
[3] Y. Wang, D. Chen, J. Zhang, M.-S. Balogun, P. Wang, Y. Tong, Y. Huang, *Adv. Funct. Mater.* **2022**, *32*, 2112738.
[4] Y. J. Jeong, D. H. Seo, J. H. Baek, M. J. Kang, B. N. Kim, S. K. Kim, X. Zheng, I. S. Cho, *Adv. Funct. Mater.* **2022**, *32*, 2208196.
[5] I. Y. Ahmet, Y. Ma, J.-W. Jang, T. Henschel, B. Stannowski, T. Lopes, A. Vilanova, A. Mendes, F. F. Abdi, R. van de Krol, *Sustain. Energy Fuels* **2019**, *3*, 2366.
[6] J. H. Kim, D. Hansora, P. Sharma, J.-W. Jang, J. S. Lee, *Chem. Soc. Rev.* **2019**, *48*, 1908.
[7] H. Nishiyama, T. Yamada, M. Nakabayashi, Y. Maehara, M. Yamaguchi, Y. Kuromiya, Y. Nagatsuma, H. Tokudome, S. Akiyama, T. Watanabe, R. Narushima, S. Okunaka, N. Shibata, T. Takata, T. Hisatomi, K. Domen, *Nature* **2021**, *598*, 304.
[8] J. Yang, D. Wang, H. Han, C. Li, *Acc. Chem. Res.* **2013**, *46*, 1900.
[9] A. Fujishima, K. Honda, *Nature* **1972**, *238*, 37.
[10] C. Bie, H. Yu, B. Cheng, W. Ho, J. Fan, J. Yu, *Adv. Mater.* **2021**, *33*, 2003521.
[11] A. Kudo, Y. Miseki, *Chem. Soc. Rev.* **2009**, *38*, 253.
[12] H. Suzuki, H. Kunioku, M. Higashi, O. Tomita, D. Kato, H. Kageyama, R. Abe, *Chem. Mater.* **2018**, *30*, 5862.
[13] L. An, M. Kitta, A. Iwase, A. Kudo, N. Ichikuni, H. Onishi, *ACS Catal.* **2018**, *8*, 9334.
[14] B. C. M. Martindale, G. A. M. Hutton, C. A. Caputo, E. Reisner, *J. Am. Chem. Soc.* **2015**, *137*, 6018.
[15] J. Willkomm, K. L. Orchard, A. Reynal, E. Pastor, J. R. Durrant, E. Reisner, *Chem. Soc. Rev.* **2016**, *45*, 9.
[16] A. Galushchinskiy, C. Pulignani, H. Szalad, E. Reisner, J. Albero, N. V. Tarakina, C. M. Pelicano, H. García, O. Savateev, M. Antonietti, *Sol. RRL* **2023**, *7*, 2300077. https://doi.org/10.1002/solr.202300077
[17] Y. Sasaki, H. Kato, A. Kudo, *J. Am. Chem. Soc.* **2013**, *135*, 5441.
[18] J. S. Chen, C. Chen, J. Liu, R. Xu, S. Z. Qiao, X. W. Lou, *Chem. Commun.* **2011**, *47*, 2631.
[19] B. Samanta, Á. Morales-García, F. Illas, N. Goga, J. A. Anta, S. Calero, A. Bieberle-Hütter, F. Libisch, A. B. Muñoz-García, M. Pavone, M. Caspary Toroker, *Chem. Soc. Rev.* **2022**, *51*, 3794.
[20] I. Samriti, I. Manisha, Z. Chen, S. Sun, J. Prakash, *Mol Syst Des Eng***2022**, *7*, 213.
[21] D. Yazaki, T. Kawawaki, T. Tanaka, D. Hirayama, Y. Shingyouchi, Y. Negishi, *Energy Adv***2023**, *2*, 1148.
[22] T. Shinagawa, Z. Cao, L. Cavallo, K. Takanabe, *J. Energy Chem.* **2017**, *26*, 259.
[23] J. Yu, B. Yang, B. Cheng, *Nanoscale* **2012**, *4*, 2670.
[24] F. Wen, X. Wang, L. Huang, G. Ma, J. Yang, C. Li, *ChemSusChem* **2012**, *5*, 849.
[25] K. Chang, X. Hai, J. Ye, *Adv. Energy Mater.* **2016**, *6*, 1502555.
[26] Y. Liu, Z. Sun, Y. H. Hu, *Chem. Eng. J.* **2021**, *409*, 128250.
[27] K. Domen, S. Naito, M. Soma, T. Onishi, K. Tamaru, *J. Chem. Soc. Chem. Commun.* **1980**, 543. https://doi.org/10.1039/C39800000543
[28] Y. Goto, T. Hisatomi, Q. Wang, T. Higashi, K. Ishikiriyama, T. Maeda, Y. Sakata, S. Okunaka, H. Tokudome, M. Katayama, S. Akiyama, H. Nishiyama, Y. Inoue, T. Takewaki, T. Setoyama, T. Minegishi, T. Takata, T. Yamada, K. Domen, *Joule* **2018**, *2*, 509.
[29] F. Xue, Y. Si, M. Wang, M. Liu, L. Guo, *Nano Energy* **2019**, *62*, 823.
[30] L. Mu, Y. Zhao, A. Li, S. Wang, Z. Wang, J. Yang, Y. Wang, T. Liu, R. Chen, J. Zhu, F. Fan, R. Li, C. Li, *Energy Environ. Sci.* **2016**, *9*, 2463.
[31] X. Ning, J. Li, B. Yang, W. Zhen, Z. Li, B. Tian, G. Lu, *Appl. Catal., B* **2017**, *212*, 129.
[32] T. Zhang, X. Lan, L. Wang, J. Shi, K. Xiao, *Catal. Sci. Technol.* **2022**, *12*, 935.
[33] R. Boppella, C. H. Choi, J. Moon, D. Ha Kim, *Appl. Catal., B* **2018**, *239*, 178.
[34] T. Ikeda, A. Xiong, T. Yoshinaga, K. Maeda, K. Domen, T. Teranishi, *J. Phys. Chem. C* **2013**, *117*, 2467.
[35] C. M. Pelicano, M. Saruyama, R. Takahata, R. Sato, Y. Kitahama, H. Matsuzaki, T. Yamada, T. Hisatomi, K. Domen, T. Teranishi, *Adv. Funct. Mater.* **2022**, *32*, 2202987.
[36] W. Kurashige, Y. Mori, S. Ozaki, M. Kawachi, S. Hossain, T. Kawawaki, C. J. Shearer, A. Iwase, G. F. Metha, S. Yamazoe, A. Kudo, Y. Negishi, *Angew. Chem. Int. Ed.* **2020**, *59*, 7076.
[37] S. Das, A. Jangam, Y. Du, K. Hidajat, S. Kawi, *Chem. Commun.* **2019**, *55*, 6074.
[38] J. Cho, L. Xu, C. Jo, R. Ryoo, *Chem. Commun.* **2017**, *53*, 3810.
[39] X. Zhang, M. Gao, L. Qiu, J. Sheng, W. Yang, Y. Yu, *J. Energy Chem.* **2023**, *79*, 64.
[40] K. Wenderich, G. Mul, *Chem. Rev.* **2016**, *116*, 14587.
[41] S. Sun, L. He, M. Yang, J. Cui, S. Liang, *Adv. Funct. Mater.* **2022**, *32*, 2106982.
[42] G. Ma, J. Liu, T. Hisatomi, T. Minegishi, Y. Moriya, M. Iwase, H. Nishiyama, M. Katayama, T. Yamada, K. Domen, *Chem. Commun.* **2015**, *51*, 4302.
[43] D. H. K. Murthy, H. Matsuzaki, Z. Wang, Y. Suzuki, T. Hisatomi, K. Seki, Y. Inoue, K. Domen, A. Furube, *Chem. Sci.* **2019**, *10*, 5353.
[44] S. Chen, S. Nandy, J. J. M. Vequizo, T. Hisatomi, M. Nakabayashi, Z. Pan, Q. Xiao, Z. Wang, L. Lin, S. Sun, K. Kato, A. Yamakata, N. Shibata, T. Takata, F. Zhang, K. Domen, *ACS Catal.* **2023**, *13*(5), 3285.
[45] Z. Wang, J. Fan, B. Cheng, J. Yu, J. Xu, *Mater. Today Phys.***2020**, *15*, 100279.
[46] B. Tahir, M. Tahir, *Appl. Surf. Sci.* **2020**, *506*, 145034.
[47] T. Kotani, K. Ogawa, H. Suzuki, K. Kato, O. Tomita, A. Yamakata, R. Abe, *EES Catal.* **2023**, *1*, 255. https://doi.org/10.1039/D2EY00109H
[48] E. M. See, C. Tossi, L. Hällström, I. Tittonen, *ACS Omega* **2020**, *5*, 10671.
[49] H. Lyu, T. Hisatomi, Y. Goto, M. Yoshida, T. Higashi, M. Katayama, T. Takata, T. Minegishi, H. Nishiyama, T. Yamada, Y. Sakata, K. Asakura, K. Domen, *Chem. Sci.* **2019**, *10*, 3196.
[50] P. Madhusudan, R. Shi, B. N. Chandrashekar, S. Xiang, A. S. Smitha, W. Wang, H. Zhang, X. Zhang, A. Amini, C. Cheng, *Adv. Mater. Interfaces* **2020**, *7*, 2000010.
[51] W. Wang, S. Zhu, Y. Cao, Y. Tao, X. Li, D. Pan, D. L. Phillips, D. Zhang, M. Chen, G. Li, H. Li, *Adv. Funct. Mater.* **2019**, *29*, 1901958.
[52] W. Y. Lim, M. Hong, G. W. Ho, *Dalton Trans.* **2016**, *45*, 552.
[53] Y. Hermans, C. Olivier, H. Junge, A. Klein, W. Jaegermann, T. Toupance, *ACS Appl. Mater. Interfaces* **2020**, *12*, 53910.
[54] F. Zhang, Y. Dong, P. Jiang, G. Wang, N. Zhao, H. Zhang, D. Li, J. Lyu, Y. Wang, J. Li, Y. Zhu, *Chem. Asian J.* **2019**, *14*, 4193.
[55] Z. Guo, H. Hou, J. Zhang, P. Cai, J. Lin, *RSC Adv.* **2021**, *11*, 12442.
[56] K.-Q. Lu, M.-Y. Qi, Z.-R. Tang, Y.-J. Xu, *Langmuir* **2019**, *35*, 11056.
[57] R. L. Lee, P. D. Tran, S. S. Pramana, S. Y. Chiam, Y. Ren, S. Meng, L. H. Wong, J. Barber, *Catal. Sci. Technol.* **2013**, *3*, 1694.
[58] J. Xu, W. Zhong, H. Yu, X. Hong, J. Fan, J. Yu, *J. Mater. Chem. C* **2020**, *8*, 15816.
[59] Y. Dong, L. Kong, P. Jiang, G. Wang, N. Zhao, H. Zhang, B. Tang, *ACS Sustain. Chem. Eng.* **2017**, *5*, 6845.

[60] L. Yang, L. Zeng, H. Liu, Y. Deng, Z. Zhou, J. Yu, H. Liu, W. Zhou, *Appl. Catal., B* **2019**, *249*, 98.
[61] C. Han, Y. Lu, J. Zhang, L. Ge, Y. Li, C. Chen, Y. Xin, L. Wu, S. Fang, *J. Mater. Chem. A* **2015**, *3*, 23274.
[62] Y. Zhu, A. Marianov, H. Xu, C. Lang, Y. Jiang, *ACS Appl. Mater. Interfaces* **2018**, *10*, 9468.
[63] X. Li, H. Xu, Q. Luo, S. Kang, L. Qin, G. Li, J. Yang, *Sustain. Energy Fuels*, **2017**, *1*, 548–554.
[64] A. Meng, W. Tian, H. Yang, X. Wang, X. Wang, Z. Li, *J. Hazard. Mater.* **2021**, *413*, 125400.
[65] M. Hu, J. Zhu, W. Guo, Q. Xu, Y. Min, J. Fan, *ACS Sustain. Chem. Eng.* **2022**, *10*, 1008.
[66] M. Saruyama, C. M. Pelicano, T. Teranishi, *Chem. Sci.* **2022**, *13*, 2824.
[67] T. Kawawaki, Y. Kataoka, M. Hirata, Y. Akinaga, R. Takahata, K. Wakamatsu, Y. Fujiki, M. Kataoka, S. Kikkawa, A. S. Alotabi, S. Hossain, D. J. Osborn, T. Teranishi, G. G. Andersson, G. F. Metha, S. Yamazoe, Y. Negishi, *Angew. Chem. Int. Ed.* **2021**, *60*, 21340.
[68] N. Sakamoto, H. Ohtsuka, T. Ikeda, K. Maeda, D. Lu, M. Kanehara, K. Teramura, T. Teranishi, K. Domen, *Nanoscale* **2009**, *1*, 106.
[69] Y. Yamada, T. Miyahigashi, H. Kotani, K. Ohkubo, S. Fukuzumi, *Energy Environ. Sci.* **2012**, *5*, 6111.
[70] J. Yu, J. Ran, *Energy Environ. Sci.* **2011**, *4*, 1364.
[71] J. Zhang, M. Grzelczak, Y. Hou, K. Maeda, K. Domen, X. Fu, M. Antonietti, X. Wang, *Chem. Sci.* **2012**, *3*, 443.
[72] C. T. Dinh, M. H. Pham, F. Kleitz, T. O. Do, *J. Mater. Chem. A* **2013**, *1*, 13308.
[73] H. Kato, K. Asakura, A. Kudo, *J. Am. Chem. Soc.* **2003**, *125*, 3082.
[74] F. Yang, Q. Zhang, Y. Liu, S. Chen, *J. Phys. Chem. C* **2011**, *115*, 19311.
[75] T. L. Tan, L.-L. Wang, D. D. Johnson, K. Bai, *Nano Lett.* **2012**, *12*, 4875.
[76] T. L. Tan, L. L. Wang, J. Zhang, D. D. Johnson, K. Bai, *ACS Catal.* **2015**, *5*, 2376.
[77] D. Wang, Z.-P. Liu, W.-M. Yang, *ACS Catal.* **2018**, *8*, 7270.
[78] Y. Negishi, Y. Matsuura, R. Tomizawa, W. Kurashige, Y. Niihori, T. Takayama, A. Iwase, A. Kudo, *J. Phys. Chem. C* **2015**, *119*, 11224.
[79] S. Cao, J. Jiang, B. Zhu, J. Yu, *Phys. Chem. Chem. Phys.* **2016**, *18*, 19457.
[80] K. D. Gilroy, A. Ruditskiy, H.-C. Peng, D. Qin, Y. Xia, *Chem. Rev.* **2016**, *116*, 10414.
[81] J. Meng, B. Zhu, Y. Gao, *J. Phys. Chem. C* **2019**, *123*, 28241.
[82] K. Chen, J. Xiao, J. J. M. Vequizo, T. Hisatomi, Y. Ma, M. Nakabayashi, T. Takata, A. Yamakata, N. Shibata, K. Domen, *J. Am. Chem. Soc.* **2023**, *145*(7), 3839.
[83] S. Zong, L. Tian, X. Guan, C. Cheng, J. Shi, L. Guo, *J. Colloid Interface Sci.* **2022**, *606*, 491.
[84] Z. W. Seh, J. Kibsgaard, C. F. Dickens, I. Chorkendorff, J. K. Nørskov, T. F. Jaramillo, *Science* **2017**, *355*, 6321.
[85] K. Yamaguti, S. Sato, *J. Chem. Soc., Faraday Trans. 1* **1985**, *81*, 1237.
[86] K. Maeda, K. Teramura, D. Lu, N. Saito, Y. Inoue, K. Domen, *Angew. Chem. Int. Ed.* **2006**, *45*, 7806.
[87] M. Yoshida, K. Takanabe, K. Maeda, A. Ishikawa, J. Kubota, Y. Sakata, Y. Ikezawa, K. Domen, *J. Phys. Chem. C* **2009**, *113*, 10151.
[88] T. Ohno, L. Bai, T. Hisatomi, K. Maeda, K. Domen, *J. Am. Chem. Soc.* **2012**, *134*, 8254.
[89] T. H. Chiang, H. Lyu, T. Hisatomi, Y. Goto, T. Takata, M. Katayama, T. Minegishi, K. Domen, *ACS Catal.* **2018**, *8*, 2782.
[90] Z. Wang, Y. Inoue, T. Hisatomi, R. Ishikawa, Q. Wang, T. Takata, S. Chen, N. Shibata, Y. Ikuhara, K. Domen, *Nat. Catal.* **2018**, *1*, 756.
[91] Q. Wang, M. Nakabayashi, T. Hisatomi, S. Sun, S. Akiyama, Z. Wang, Z. Pan, X. Xiao, T. Watanabe, T. Yamada, N. Shibata, T. Takata, K. Domen, *Nat. Mater.* **2019**, *18*, 827.
[92] A. T. Garcia-Esparza, T. Shinagawa, S. Ould-Chikh, M. Qureshi, X. Peng, N. Wei, D. H. Anjum, A. Clo, T.-C. Weng, D. Nordlund, D. Sokaras, J. Kubota, K. Domen, K. Takanabe, *Angew. Chem. Int. Ed.* **2017**, *56*, 5780.
[93] T. Higashi, K. Seki, Y. Sasaki, Y. Pihosh, V. Nandal, M. Nakabayashi, N. Shibata, K. Domen, *Chem. - Eur. J.* **2023**, *29*, e202204058.
[94] T. Takata, C. Pan, M. Nakabayashi, N. Shibata, K. Domen, *J. Am. Chem. Soc.* **2015**, *137*, 9627.
[95] Y. P. Xie, G. Liu, L. Yin, H. M. Cheng, *J. Mater. Chem.* **2012**, *22*, 6746.
[96] G. Liu, J. C. Yu, G. Q. Lu, H. M. Cheng, *Chem. Commun.* **2011**, *47*, 6763.
[97] T. Takata, J. Jiang, Y. Sakata, M. Nakabayashi, N. Shibata, V. Nandal, K. Seki, T. Hisatomi, K. Domen, *Nature* **2020**, *581*, 411.
[98] A. Indra, P. W. Menezes, K. Kailasam, D. Hollmann, M. Schröder, A. Thomas, A. Brückner, M. Driess, *Chem. Commun.* **2016**, *52*, 104.
[99] Y. H. Li, C. Li, H. G. Yang, *J. Mater. Chem. A* **2017**, *5*, 20631.
[100] D. Spanu, A. Minguzzi, S. Recchia, F. Shahvardanfard, O. Tomanec, R. Zboril, P. Schmuki, P. Ghigna, M. Altomare, *ACS Catal.* **2020**, *10*, 8293.
[101] B. Mei, K. Han, G. Mul, *ACS Catal.* **2018**, *8*, 9154.
[102] I. Ivanova, T. A. Kandiel, Y.-J. Cho, W. Choi, D. Bahnemann, *ACS Catal.* **2018**, *8*, 2313.
[103] X.-P. Wu, I. Choudhuri, D. G. Truhlar, *Energy Environ. Mater.* **2019**, *2*, 251.
[104] Y. Zheng, Y. Jiao, M. Jaroniec, S. Z. Qiao, *Angew. Chem. Int. Ed.* **2015**, *54*, 52.
[105] D. Gao, W. Zhong, X. Wang, F. Chen, H. Yu, *J. Mater. Chem. A* **2022**, *10*, 7989.
[106] J. Ran, G. Gao, F.-T. Li, T.-Y. Ma, A. Du, S.-Z. Qiao, *Nat. Commun.* **2017**, *8*, 13907.
[107] Y. H. Li, C. Peng, S. Yang, H. F. Wang, H. G. Yang, *J. Catal.* **2015**, *330*, 120.
[108] W. Sheng, M. Myint, J. G. Chen, Y. Yan, *Energy Environ. Sci.* **2013**, *6*, 1509.

How to cite this article: C. M. Pelicano, H. Tong, *Appl. Res.* **2024**;*3*:e202300080. https://doi.org/10.1002/appl.202300080